JACS JOURNAL OF THE AMERICAN CHEMICAL SOCIETY

Article

Cite This: J. Am. Chem. Soc. 2019, 141, 19118−19129

pubs.acs.org/JACS

Accelerating the Shuttling in Hydrogen-Bonded Rotaxanes: Active Role of the Axle and the End Station

Tatu Kumpulainen,*[,†] Matthijs R. Panman,[‡] Bert H. Bakker, Michiel Hilbers, Sander Woutersen,* and Albert M. Brouwer*

Van't Hoff Institute for Molecular Sciences, Faculty of Science, University of Amsterdam, P.O. Box 94157, 1090 GD Amsterdam, The Netherlands

Supporting Information

ABSTRACT: The relation between the chemical structure and the mechanical behavior of molecular machines is of paramount importance for a rational design of superior nanomachines. Here, we report on a mechanistic study of a nanometer scale translational movement in two bistable rotaxanes. Both rotaxanes consist of a tetra-amide macrocycle interlocked onto a polyether axle. The macrocycle can shuttle between an initial succinamide station and a 3,6-dihydroxy- or 3,6-di-*tert*-butyl-1,8-naphthalimide end stations. Translocation of the macrocycle is controlled by a hydrogen-bonding equilibrium between the stations. The equilibrium can be perturbed photochemically by either intermolecular proton or electron transfer depending on the system. To the best of our knowledge, utilization of proton transfer from a conventional photoacid for the operation of a molecular machine is demonstrated for the first time. The shuttling dynamics are monitored by means of UV−vis and IR transient absorption spectroscopies. The polyether axle accelerates the shuttling by ∼70% compared to a structurally similar rotaxane with an all-alkane thread of the same length. The acceleration is attributed to a decrease in activation energy due to an early transition state where the macrocycle partially hydrogen bonds to the ether group of the axle. The dihydroxyrotaxane exhibits the fastest shuttling speed over a nanometer distance ($\tau_{shuttling} \approx 30$ ns) reported to date. The shuttling in this case is proposed to take place via a so-called harpooning mechanism where the transition state involves a folded conformation due to the hydrogen-bonding interactions with the hydroxyl groups of the end station.

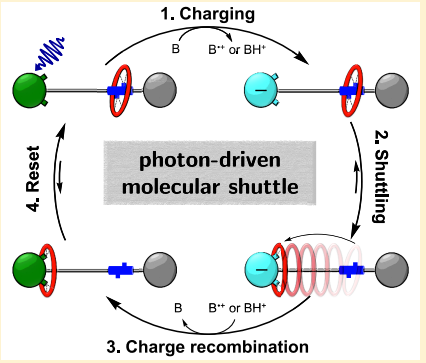

INTRODUCTION

The control of motion on a molecular scale is one of the great challenges in present-day nanotechnology. This has led to a rapid development of mechanically interlocked molecules designed to perform a specific function in response to external stimuli.[1−12] Rotaxanes constitute one of the best-studied classes of such molecules due to their potential applications in molecular switches[13−16] and machines.[17−22] [2]Rotaxanes are composed of a molecular wheel (macrocycle) that is mechanically interlocked onto a molecular axle (thread) by bulky stoppers. Rotaxanes often contain two or more recognition sites (stations), and the macrocycle can shuttle along the thread between these stations.[23−25]

Contrary to their macroscopic counterparts, the components of the molecular machines are in perpetual random motion due to thermal fluctuations.[26,27] Therefore, the supplied energy, often in the form of chemical,[28−33] electrochemical,[34−36] or photochemical input,[37−41] is used to drive the system temporarily out of equilibrium and bias the movement of the macrocycle to one direction.[42,43] Light activation offers a clean energy supply without formation of byproducts and the possibility to convert solar energy directly into mechanical work. In addition, light-induced molecular motion combined with optical monitoring by means of time-resolved laser spectroscopy offers a superior time resolution for detailed kinetic studies. Examples of photochemical reactions used for the operation of [2]rotaxanes include photoinduced isomerization[44−46] and electron transfer,[47,48] but to the best of our knowledge, excited-state proton transfer has not yet been utilized for this purpose.[49]

Despite the large number of molecular machines reported in the literature,[6,19] few studies are aimed at elucidating the working principles and the factors influencing nanoscale motion.[50−54] In particular, detailed kinetic studies of fast shuttling processes are scarce.[55−58] The effect of the solvent,[47,56,59] axle length,[55,60] and hydrogen-bonding stations[57,61] in a series of bistable hydrogen-bonded [2]rotaxanes has led to the proposition of two different shuttling mechanisms. In an earlier work, the overall shuttling was modeled as a two-step process: escape from the initial station followed by a biased random walk motion along the axle, which could explain the decrease in the shuttling rate upon increasing axle length.[55] Contrary to the biased random walk model, Hirose et al. did not find any effect of the axle length, in this case a rigid axle, on the shuttling rate.[54] Axle-length

Received: September 16, 2019
Published: November 7, 2019

DOI: 10.1021/jacs.9b10005
J. Am. Chem. Soc. 2019, 141, 19118−19129

independent shuttling rates were also recently reported for both rigid and flexible spacers.[62,63] Another study proposed a "harpooning" mechanism in which the macrocycle is hydrogen bonded simultaneously to both stations in the transition state.[57] Jeppesen and Flood et al. also proposed that longer linkers facilitate folding of the rotaxanes, enabling simultaneous interactions between the macrocycle and both of the stations.[53] Second, the authors proposed that a polyether axle plays an active role in the shuttling process via interactions with the macrocycle.

Most of the rotaxanes previously studied in our group were composed of a 3,6-di-*tert*-butyl-1,8-naphthalimide (***t*Bu-NI**) end station, a succinamide initial station (**succ**), an alkane thread, and a tetra-amide macrocycle (**mc**). In the present study, the alkane thread has been replaced with a polyether chain (**PE**, C_6O_2) to investigate whether the hydrogen-bonding capability of the thread plays an active role in the shuttling process. In addition, the **PE** thread has been combined with the 3,6-di-*tert*-butyl-1,8-naphthalimide and a novel 3,6-dihydroxy-1,8-naphthalimide (**dOH-NI**) end stations (Chart 1) to specifically study the effect of the different end

Chart 1. Structures of the Studied Compounds[a]

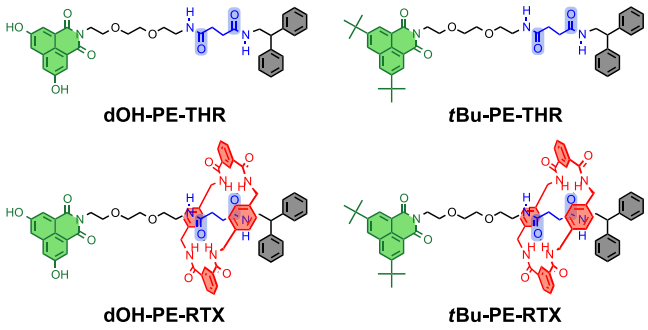

[a]Abbreviations used throughout the text: **dOH-NI** = 3,6-dihydroxy-1,8-naphthalimide, ***t*Bu-NI** = 3,6-di-*tert*-butyl-1,8-naphthalimide, **PE** = polyether (C_6O_2), **THR** = thread, and **RTX** = rotaxane.

stations on the shuttling rate. Our results identify several key factors that can be utilized to accelerate the shuttling motion and can aid in the design of superior nanomachines.

The proposed shuttling mechanism for both rotaxanes is based on a hydrogen-bonding (HB) equilibrium between the macrocycle and the two stations. The HB affinities are illustrated by the potential wells in Scheme 1, with colors corresponding to those of the stations. In the neutral state, the HB affinity of the **mc** is higher toward the **succ** station, and the **mc** resides predominantly (>99%) on the initial **succ** station.[47,55] The HB affinity, that is, the depth of the potential well, of the **mc** toward the **dOH-NI** or the ***t*Bu-NI** end station can be changed by increasing the negative charge of the chromophores (step 1, Charging). This is achieved in two different ways. In the case of **dOH-PE-RTX**, a weak base acts as a proton acceptor, and excitation of the photoacidic **dOH-NI** unit results in a rapid (sub-nanosecond) proton transfer and eventually to a formation of the ground-state deprotonated anion of the **dOH-NI** end station.[64] In the case of ***t*Bu-PE-RTX**, excitation of the ***t*Bu-NI** unit results in a rapid intersystem crossing to the triplet state followed by an intermolecular electron transfer from an electron donor to produce the ***t*Bu-NI** radical anion. In both cases, the HB affinity of the macrocycle toward the **NI** unit is increased, and

Scheme 1. Proposed Photoinduced Working Cycle of the [2]Rotaxane-Based Molecular Machines[a]

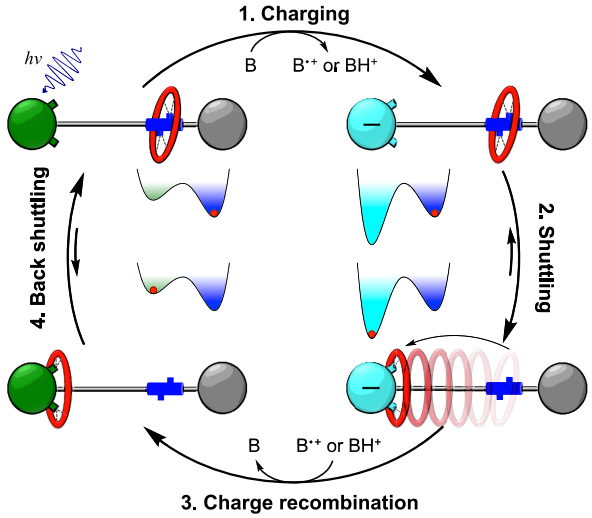

[a]Hydrogen-bonding affinities of the **mc** (red) to the **succ** (dark blue) and the **NI** (green = neutral and light blue = anionic) stations are illustrated by the potential wells in the middle of the scheme. Excitation of the **NI** station in the presence of a weak base (proton acceptor/electron donor) results in either intermolecular excited-state proton or electron transfer to produce the ground-state (radical) anion. Shuttling takes place due to the increased hydrogen-bonding affinity to the anionic end station. Spontaneous bimolecular charge recombination eventually produces the neutral **NI** station on a microsecond time scale after which the back shuttling takes place, completing the photocycle.

shuttling takes place to reach the new equilibrium (step 2, Shuttling). The produced ions spontaneously recombine on a ~100 μs time scale, yielding the neutral **NI** station and regenerating the base (step 3, Charge recombination). The HB affinities are restored, and the macrocycle shuttles back and rebinds the **succ** station, completing the photocycle (step 4, Back shuttling). Consequently, the system is reset to the initial state and ready for a new cycle without the need to replenish or add additional reagents.

An important advantage of using the proton transfer as a mechanism for the charging step is the much faster time scale of the reaction. Initial deprotonation in a preformed ground-state complex of the **dOH-NI** unit and a weak base takes place on a sub-nanosecond time scale,[64] whereas the bimolecular electron transfer is dependent on the concentration of the electron donor and can take up to several tens of nanoseconds.[55] The charging and shuttling dynamics can become indistinguishable if they occur on similar time scales.

The article is structured as follows. First, we will treat the steady-state characterization of **dOH-PE-RTX** and **dOH-PE-THR** upon addition of weak (*N*-methyl imidazole, NMI) and strong (1,8-diazabicyclo[5.4.0]undec-7-ene, DBU) bases in polar organic solvents, acetonitrile (MeCN) and benzonitrile (PhCN). The association constants are compared to those obtained with the *N*-butyl-substituted model compound, **ref-dOHNI**, and the effects of the macrocycle on the spectral and acid−base properties of the **dOH-NI** unit are discussed. Second, we present the excited-state proton transfer (ESPT)-induced shuttling experiments of the **dOH-PE-RTX** rotaxane in the presence of a weak base, NMI or 1,4-diazabicyclo[2.2.2]-octane (DABCO), in the visible and IR spectral region. Third,

DOI: 10.1021/jacs.9b10005
J. Am. Chem. Soc. 2019, 141, 19118−19129

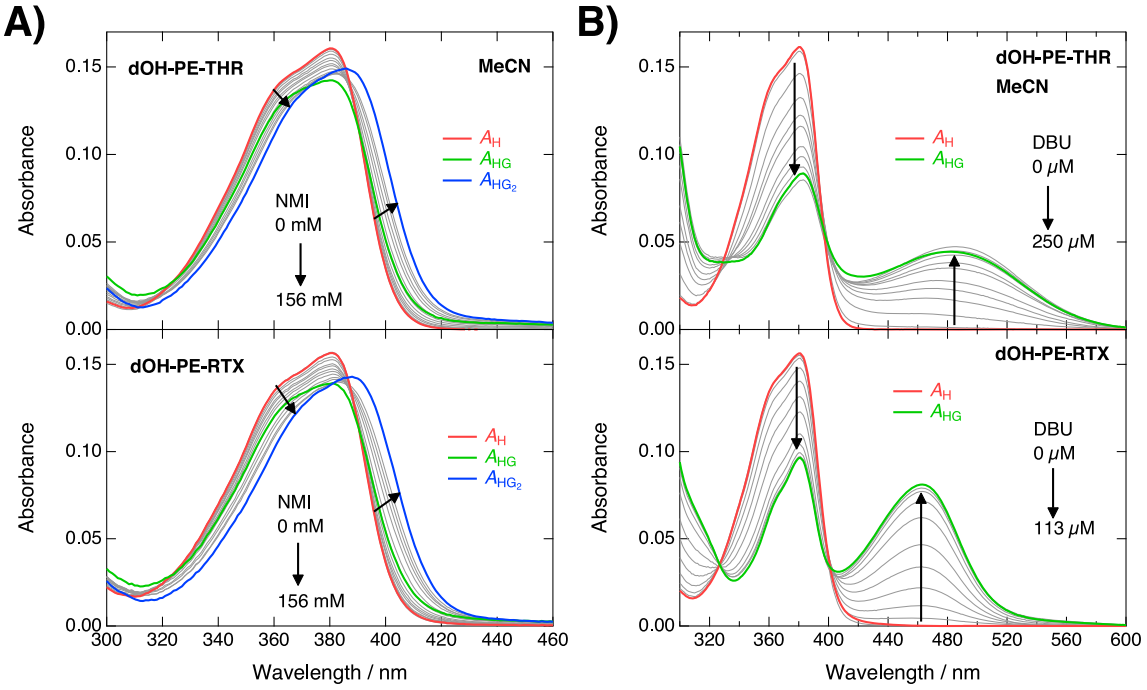

Figure 1. Steady-state absorption spectra of (top) **dOH-PE-THR** and (bottom) **dOH-PE-RTX** ($c \approx 15$ μM) upon addition of (A) NMI and (B) DBU in MeCN. The absorption of the bases has been subtracted from the overall absorption spectra. The colored solid lines represent the spectra of the pure species obtained from the global fits.

we describe the shuttling experiments of ***t*Bu-PE-RTX** using DABCO as the electron donor. The photophysical properties of ***t*Bu-NI**-based rotaxanes are well-described in the existing literature[47,65,66] and will not be discussed in detail here. Finally, we will compare our results with those obtained with a rotaxane based on an all-alkane axle and discuss the effect of the composition of the thread and the end station to the shuttling rate and mechanism.

RESULTS

UV−Vis Experiments on dOH-PE-THR and dOH-PE-RTX. We have shown in a previous publication[64] that weak bases form neutral ground-state complexes with the hydroxyl groups of the **dOH-NI** unit that undergo a rapid ESPT upon excitation. According to the proposed operation mechanism of the dihydroxyrotaxane, the shuttling in this case is expected to occur only via the excited-state pathway. Strong bases, on the other hand, are able to deprotonate one of the hydroxyl groups in the ground state, but the protonated base remains hydrogen bonded to the deprotonated hydroxyl oxygen. If the interaction of the macrocycle toward the deprotonated **dOH-NI** unit is significantly stronger than that of the protonated DBU, strong bases are expected to result in translocation of the macrocycle already in the ground state. The shuttling is additionally expected to increase the acidity of the hydroxyl group due to the additional stabilization of deprotonated **dOH-NI** by the macrocycle. The absorption spectra of **dOH-PE-THR** and **dOH-PE-RTX** upon addition of a weak (NMI) and a strong base (DBU) in MeCN and PhCN are presented in Figures 1 and S4 (Supporting Information), respectively.

The absorption spectra of the rotaxane and the thread exhibit a red shift and a broadening upon addition of NMI. The spectra were analyzed globally with a 1:2 host/guest association model assuming noncooperative binding (i.e., $K_1 = 4K_2$; see Supporting Information for additional details, spectra, and fits),[64] and the association constants are summarized in Table 1. The obtained species spectra for the free host (A_H), 1:1 complex (A_{HG}), and 1:2 complex (A_{HG_2}) are depicted in Figure 1 by the colored lines. The association constants of both compounds are slightly smaller than those of the model compound, **ref-dOHNI**, which could indicate some competition in the binding of NMI toward the initial succ station or the macrocycle.[64] The spectral changes are similar in all cases. Nevertheless, formation of the ground-state complexes between the **dOH-NI** unit and NMI is not significantly influenced by the presence of the thread or the macrocycle.

Table 1. Association Constants for Complex Formation between the Dihydroxy Compounds and NMI and the Equilibrium Constant for Deprotonation by DBU

compound[a]	solvent	base	K_1 (M^{-1})	K_2 (M^{-1})
THR			50 ± 3	12 ± 1
RTX	MeCN	NMI	55 ± 4	14 ± 1
ref-dOHNI			58 ± 10[b]	9 ± 2[b]
THR			73 ± 6	18 ± 2
RTX	PhCN	NMI	83 ± 6	21 ± 2
ref-dOHNI			95 ± 9[b]	19 ± 2[b]
THR			$(1.8 \pm 0.1) \times 10^5$	
RTX	MeCN	DBU	$(5.5 \pm 0.2) \times 10^5$	
ref-dOHNI			$(1.9 \pm 0.1) \times 10^{5}$[b]	
THR			$(2.1 \pm 0.4) \times 10^4$	
RTX	PhCN	DBU	$(9.6 \pm 0.7) \times 10^5$	
ref-dOHNI			$(4.1 \pm 0.2) \times 10^{4}$[b]	

[a]**THR** = **dOH-PE-THR**; **RTX** = **dOH-PE-RTX**. [b]Values taken from ref 64.

The absorption spectra upon addition of DBU exhibit a drastic decrease in the absorption band of the neutral form with a concomitant rise of a new long-wavelength absorption

DOI: 10.1021/jacs.9b10005
J. Am. Chem. Soc. 2019, 141, 19118−19129

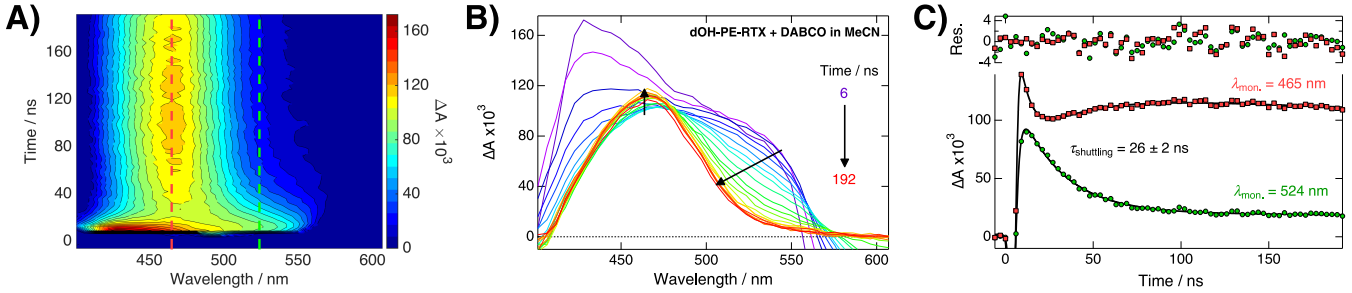

Figure 2. (A) Time-resolved UV−vis transient absorption spectra of **dOH-PE-RTX** ($c \approx 100$ μM) in the presence of DABCO ($c = 60$ mM) in MeCN. Negative intensities due to emissive processes are removed for clarity. (B) 2D representation of the same spectra. (C) Decays monitored at 465 nm (red squares) and 524 nm (green circles) together with multiexponential fits (black solid lines). The residuals are given in the top panel. The excitation wavelength was 385 nm.

band attributed to the 1:1 complex of the ground-state ion pair (deprotonated **dOH-NI** + protonated DBU). Clear changes are observed between the thread and the rotaxane. First, the rotaxane responds much more readily to the addition of DBU (notice the different concentration ranges in Figure 1B). Second, the spectrum of the ground-state anion of the rotaxane is significantly blue-shifted (463 nm vs 486 nm in MeCN), narrower and higher in intensity. The differences must originate from the presence of the macrocycle. We have shown in a previous publication that hydrogen-bonding interactions to deprotonated hydroxyl oxygen atoms in related 1,8-naphthalimide photoacids greatly stabilize the ground-state anion, causing a blue shift of the spectrum.[64,67] The blue shift observed for the rotaxane suggests that the macrocycle stabilizes the ground-state anion of **dOH-NI** presumably via hydrogen bonding to the deprotonated hydroxyl oxygen. Moreover, the narrowing of the band could be due to exclusion of the solvent around the **dOH-NI** station by the macrocycle in the shuttled state. We expect to observe similar spectral changes upon shuttling of the macrocycle in the time-resolved experiments.

To quantify the observed differences between the thread and the rotaxane, the spectra upon addition of DBU were analyzed with a modified 1:2 association model. Due to the low concentration range of DBU, the concentration of 1:2 complexes, where one DBU is associated with each of the hydroxyl groups, is very low and does not need to be considered. However, we account for a competitive association channel which presumably corresponds to a binding of one DBU molecule to the initial succ station without significant spectral changes (see Supporting Information for additional details, spectra, and fits). Hence, we only determined the equilibrium constant for the deprotonation of one of the hydroxyl group by DBU, which can be compared with the corresponding K_1 value of **ref-dOHNI**. In both solvents, K_1 of **dOH-PE-THR** is comparable to that of the reference compound. On the contrary, **dOH-PE-RTX** exhibits a significantly higher K_1 in both solvents. Similarly to the above case, this can be explained by stabilization of the ground-state anion by the macrocycle resulting in an increased equilibrium constant for deprotonation (i.e., decreased pK_a value). Similar remote control of acid−base properties has been recently reported in the case of other bistable [2]rotaxanes.[33,68]

The shuttling rates were measured using a time-resolved UV−vis transient absorption setup in the presence of weak bases, DABCO ($c = 60$ mM) and NMI ($c = 200$ mM) in MeCN and PhCN. As discussed in the previous section, weak bases form neutral ground-state complexes with the hydroxyl groups which undergo sub-nanosecond ESPT and eventually produce the ground-state anion in approximately 14 ns.[64] The shuttling is expected to occur due to the increased hydrogen-bonding affinity of the **mc** toward the deprotonated **dOH-NI** station. Based on the steady-state absorption measurements in the presence of DBU, translocation of the mc induces a significant blue shift and narrowing of the ground-state anion absorption band due to hydrogen bonding of the mc to the deprotonated hydroxyl oxygen. Representative time-resolved transient absorption spectra of **dOH-PE-RTX** in the presence of 60 mM DABCO in MeCN are presented in Figure 2. The remaining time-resolved spectra, together with the fits, are presented in the Supporting Information (Figures S23−S28).

The transient spectra of **dOH-PE-RTX** in the presence of weak bases contain both negative and positive contributions from emissive and absorptive processes, respectively (see Figure 2A,B and Figure S1 for the full spectra). Excitation of the ground-state complex results in formation of excited-state ion pair species with wavelength-dependent multiexponential dynamics.[64] We therefore focused on the broad transient absorption band of the ground-state anion formed with $\tau_{ES} \approx 14$ ns and centered initially around 500 nm. During the first 100 ns, this band undergoes a significant narrowing from the red side around 480−570 nm and an increase in intensity around 440−480 nm, in excellent agreement with the observed spectral differences between the thread and the rotaxane in the presence of DBU. Moreover, the spectral evolution observed for the rotaxane could be qualitatively reproduced either from the steady-state spectra of the thread and the rotaxane in the presence of DBU or from the transient absorption spectra of the ground-state anions (Figures S4 and S5, Supporting Information). Therefore, the observed spectral changes can be attributed to an association of the macrocycle with the deprotonated **dOH-NI** end station.

In order to disentangle several overlapping contributions, the temporal evolution was analyzed with multiexponential functions at selected wavelengths. The time constant of the shuttling (reflected in the narrowing and blue shift of the ground-state anion band) was obtained as an average of four individually fitted wavelengths (see Supporting Information for details). Two representative fits are presented in Figure 2C. The shuttling is observed as a clear decay of the signal at the long-wavelength side (524 nm, green circles) and as a slight increase around the peak maximum (465 nm, red squares). The large negative feature around $t = 0$ is due to fluorescence,

DOI: 10.1021/jacs.9b10005
J. Am. Chem. Soc. 2019, 141, 19118−19129

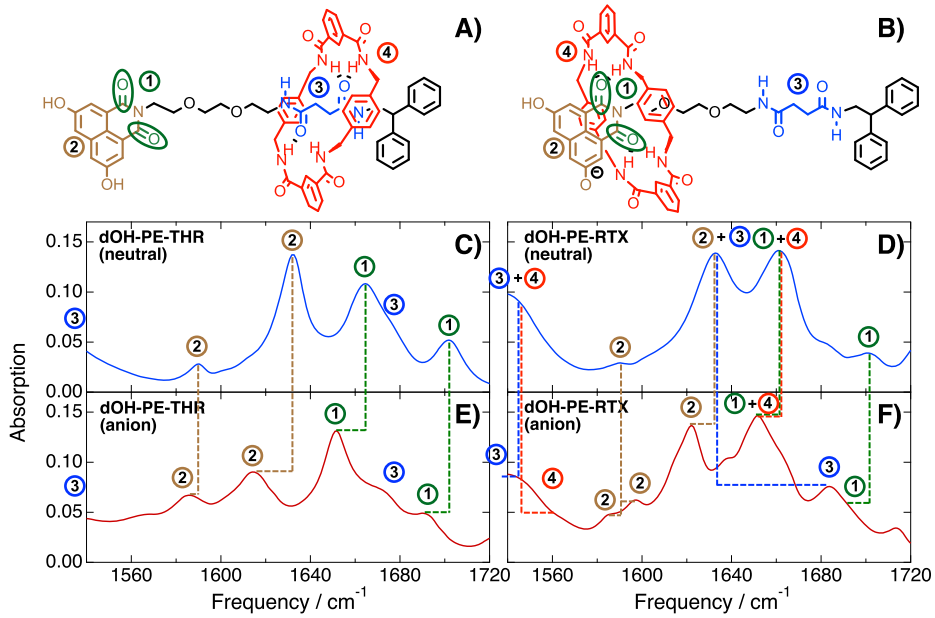

Figure 3. Example structures of the (A) neutral and (B) anionic forms of **dOH-PE-RTX**, indicating the relevant functional groups seen in the spectral window. The FTIR spectra of the (C,D) neutral and (E,F) anionic forms of (left) **dOH-PE-THR** and (right) **dOH-PE-RTX** in MeCN-d_3 together with the assignment of the relevant vibrations. The spectra of the anionic forms were measured in the presence of DBU.

whereas the fast rise at 524 nm and decay at 465 nm are mostly due to the formation and decay of the excited anionic species, respectively. In MeCN, the excited-state decay occurs on the same time scale as the shuttling process ($\tau_{shuttling}$ = 26 ns ≈ $2\tau_{ES}$), but in PhCN, these two processes are clearly distinguishable in time ($\tau_{shuttling}$ = 53 ns ≈ $4\tau_{ES}$). However, the spectral changes attributed to the shuttling are very similar in both solvents corroborating the analysis of the shuttling rates. Moreover, shuttling rates were independent of concentration and the type of the weak base in both solvents (Table S1, Supporting Information).

IR Experiments on dOH-PE-THR and dOH-PE-RTX. We performed IR experiments to obtain structural information about the species involved in the shuttling process. First, we will show the steady-state Fourier transform infrared (FTIR) spectra of the neutral and anionic forms of **dOH-PE-THR** and **dOH-PE-RTX** followed by the time-resolved UV-pump/IR-probe measurements. Due to the strong IR absorption of NMI and PhCN, we investigated the temporal behavior only in the presence of DABCO in deuterated MeCN.

The FTIR spectra of the neutral (C,D) and anionic (E,F) forms of **dOH-PE-THR** and **dOH-PE-RTX** are presented in Figure 3. Example structures of the rotaxane highlighting the most relevant functional groups observed in the spectral window are indicated in Figure 3A,B.

The spectrum of the neutral form was measured in neat MeCN-d_3 and that of the anion in the presence of DBU. Absorption of the solvent and DBU has been subtracted from the spectra. The most intense peaks in the spectral window originate from the symmetric (1702 cm^{-1}) and antisymmetric (1663 cm^{-1}) carbonyl stretch vibrations (peaks 1, green) and from the aromatic ring vibrations (1633 and 1590 cm^{-1}, peaks 2, brown) of the **dOH-NI** station.[67] In the neutral form, these vibrations are at the same frequencies for both the thread and the rotaxane. Amide I and amide II vibrations (peaks 3, blue) of the **succ** station are observed at ∼1680 and <1540 cm^{-1}, in part outside of the spectral window. In the spectrum of the rotaxane, the amide I is red-shifted and overlaps with the aromatic ring vibration, and the amide II is blue-shifted to ∼1540 cm^{-1} due to the hydrogen bonding with the **mc**. Additionally, **dOH-PE-RTX** shows the amide I and amide II vibrations (peaks 4, red) of the **mc**.[69,70]

The spectra of both compounds show large changes upon deprotonation by DBU. All major peaks of the **dOH-NI** station are shifted to lower frequencies, as indicated in Figure 3 by the dashed lines. Similar red shifts upon deprotonation (or formation of radical anion, vide infra) have been observed for related compounds and can be attributed to an increased electron density on the aromatic system.[67,69] An additional band appears at 1600 cm^{-1} in the spectrum of the rotaxane and is attributed to the aromatic ring vibration of the **dOH-NI** station. In the bare thread, the **succ** vibrations do not shift, whereas in the rotaxane, both the **succ** and the **mc** vibrations exhibit shifts. Upon deprotonation, the amide II vibration of the **succ** station is shifted outside of the spectral window, resulting in decreased absorption at 1540 cm^{-1}. The amide II vibration of the **mc** is expected to exhibit a blue shift from ∼1530 to ∼1555 cm^{-1}, but this is not clearly seen due to the overlapping contributions from other vibrations.[69] The amide I of the **succ** station is blue-shifted to 1680 cm^{-1} and overlaps with the symmetric CO-stretch vibration of the imide carbonyl. The amide I of the **mc** is red-shifted to ∼1650 cm^{-1} and overlaps with the antisymmetric CO-stretch vibration of the imide carbonyl. These changes can be attributed to the departure of the **mc** from the **succ** station and increased hydrogen-bonding strength of the **mc** to the anionic **dOH-NI** end station.[69,70] We expect to observe similar changes in our time-resolved UV−IR transient absorption experiments.

The time-resolved IR measurements were carried out with identical concentrations as the time-resolved UV−vis measurements. The samples were excited at λ_{exc} = 355 nm and monitored with mid-IR pulses over the range from 1540 to 1730 cm^{-1}. The short time scale transient IR spectra of **dOH-PE-THR** and **dOH-PE-RTX** (c ≈ 100 μM) in the presence of

DOI: 10.1021/jacs.9b10005
J. Am. Chem. Soc. 2019, 141, 19118−19129

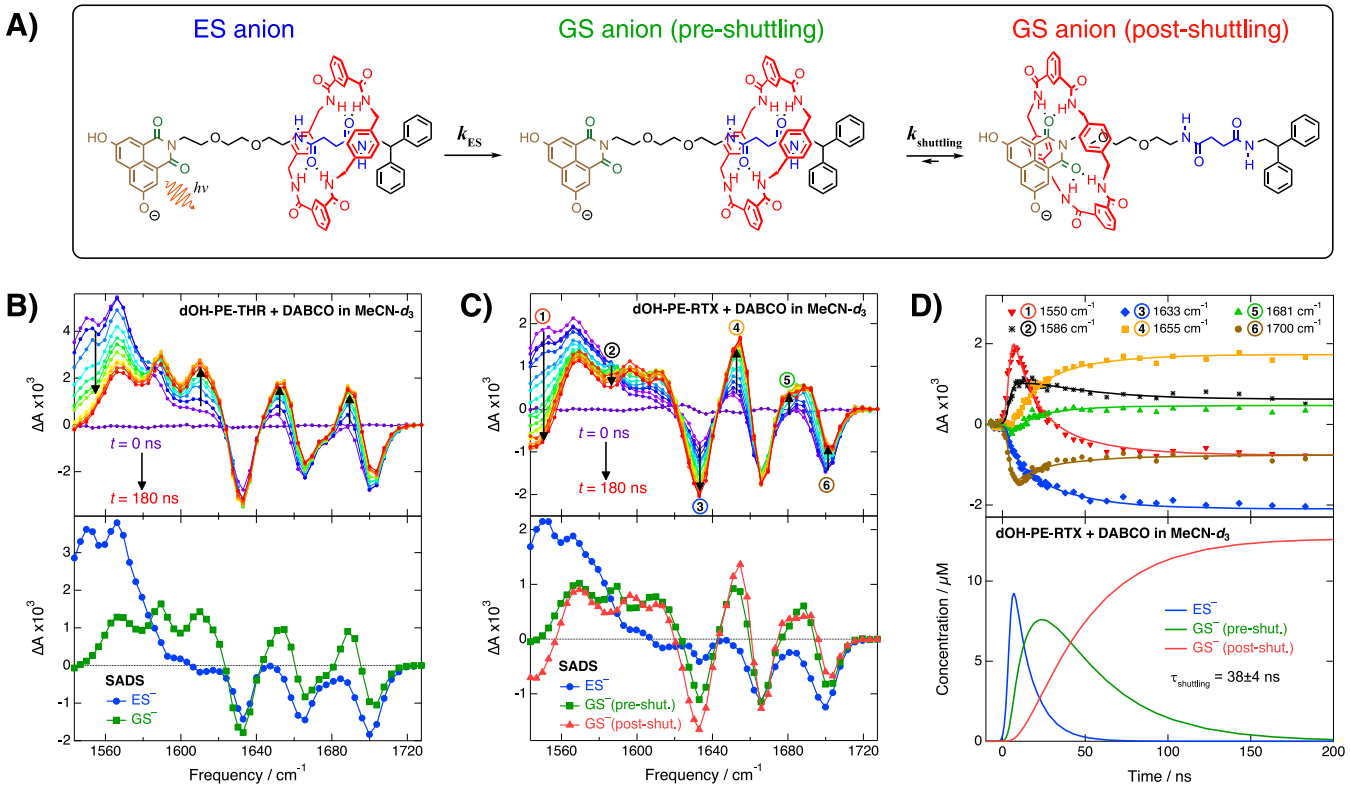

Figure 4. (A) Reaction scheme of the rotaxane following the ESPT. Time-resolved mid-IR transient absorption spectra together with the species associated difference spectra (SADS) of (B) **dOH-PE-THR** ($c \approx 100$ μM) and (C) **dOH-PE-RTX** ($c \approx 100$ μM) in the presence of DABCO (c = 60 mM) in MeCN-d_3. (D) Representative fits of the **dOH-PE-RTX** transient spectra at selected frequencies indicated in (C) and time-dependent concentrations of all the species used in the kinetic model (Supporting Information). The excitation wavelength was 355 nm.

DABCO (c = 60 mM) in MeCN-d_3 are presented in Figure 4B,C, respectively. Selected frequencies for representative fits of **dOH-PE-RTX** spectra are numbered in Figure 4C. The spectra were fitted globally with either a mono- (**dOH-PE-THR**) or a biexponential (**dOH-PE-RTX**) function combined with a bimolecular recombination and convolved with a simulated IRF with a Gaussian time profile (see Supporting Information for details).[69] The resulting species-associated difference spectra (SADS) are shown in the bottom parts of Figure 4B,C. Example fits of the rotaxane spectra and the concentration profiles of different species are presented in Figure 4D. The reaction scheme for the rotaxane is depicted in Figure 4A. Due to the sub-nanosecond ESPT, the first observed species corresponds to the excited-state anion, which is formed during the excitation pulse.

Both compounds exhibit similar spectral evolution at short delay times (<20 ns). Excitation results in bleach of the **dOH-NI** vibrations at 1633, 1663, and 1702 cm^{-1} and induced absorption below 1600 cm^{-1}. This is attributed to the formation of the excited-state anionic species within the laser pulse (~4 ns). Relaxation to the ground state during the first 20−30 ns results in blue shifts of the vibrations to the frequencies matching those determined from the FTIR spectra of the anions (Figure 3). Up to this point, the spectral evolution of the thread and the rotaxane is nearly identical as also supported by the similarity between the SADS of the first two species. After relaxation to the ground state, the transient spectra of the thread does not show any significant shifts and decays to zero due to the recombination of the ion pair. The spectra of the rotaxane, on the other hand, exhibits considerable changes: (*i*) a distinct bleach at ~1540 cm^{-1} (peak 1, red) is attributed to a red shift of the amide II vibration of the **succ** station due to the departure of the **mc**; (*ii*) the amide I vibration of the **succ** station shifts from 1633 cm^{-1} (peak 3, blue in Figure 4D) to 1681 cm^{-1} (peak 5, green), indicating a formation of the free **succ** station; (*iii*) the amide I vibration of the **mc** shifts from 1665 to 1655 cm^{-1} (peak 4, orange) due to the increased hydrogen-bonding strength of the **mc** upon arrival to the **dOH-NI** station; (*iv*) the weak band attributed to the aromatic ring vibration of the **dOH-NI** station blue shifts from 1590 cm^{-1} (peak 2, black) to 1596 cm^{-1}, which is attributed to the hydrogen bonding of the **mc** to the **dOH-NI** station. The observed shifts are in excellent agreement with the spectral shifts observed in the FTIR measurements between the thread and the rotaxane.

The SADS show the previously assigned changes more clearly at each step. The first species is assigned to the deprotonated excited-state anion (Figure 4A). The thread exhibits only two decay components which are almost identical to those of the ES anion and GS anion (preshuttling) of the rotaxane (blue and green in Figure 4B,C, respectively). The additional component of the rotaxane (red in Figure 4C) is attributed to the shuttling process and exhibits spectral features which can be attributed to departure of the **mc** from the **succ** station and hydrogen bonding to the **dOH-NI** station. The obtained time constants for the rotaxane are τ_{ES} = 12 ± 3 ns for the excited-state decay of the anion and $\tau_{shuttling}$ = 38 ± 4 ns for the shuttling process. The values are in reasonable agreement with those obtained from the UV−vis measurements (τ_{ES} = 14 ± 1 ns and $\tau_{shuttling}$ = 25 ± 4 ns). The final shuttling rates are summarized in Table 2 and represent the average values from all of the measurements (UV−vis and IR),

DOI: 10.1021/jacs.9b10005
J. Am. Chem. Soc. 2019, 141, 19118−19129

and the errors represent the corresponding standard deviations.

Table 2. Average Shuttling Time and Rate ($1/\tau_{shuttling}$) Constants of the Rotaxanes[a]

compound	solvent	$\tau_{shuttling}$ (ns)	$k_{shuttling}$ ($\times 10^7$ s^{-1})
dOH-PE-RTX	MeCN	30 ± 6	3.4 ± 0.8
***t*Bu-PE-RTX**	MeCN	160 ± 20	0.64 ± 0.08
***t*Bu-C_8-RTX**	MeCN	270 ± 30[b]	0.37 ± 0.04[b]
dOH-PE-RTX	PhCN	53 ± 5	1.9 ± 0.2
***t*Bu-PE-RTX**	PhCN	720 ± 70	0.14 ± 0.02

[a]The errors represent the standard deviations from multiple measurements (UV–vis and IR). [b]The shuttling rate as predicted by the model in ref 55.

UV–Vis and IR Experiments on *t*Bu-PE-RTX. To separate the influence of the chemical composition of the thread and the end station to the shuttling rate, we additionally investigated the shuttling dynamics in ***t*Bu-PE-RTX**. Comparison between ***t*Bu-PE-RTX** and previously investigated rotaxanes consisting of the same end station but an all-alkane spacer (***t*Bu-C_n-RTX**) allows us to investigate the effect of the **PE** thread. The shuttling was monitored by nanosecond UV–vis and IR transient absorption methods as in the case of the dihydroxyrotaxane. The data analyses are based on previously published works[47,55] and are discussed in detail in the Supporting Information. All measurements were done using DABCO (10 mM or 60 mM) as the electron donor.

Time-resolved UV–vis transient absorption spectra of ***t*Bu-PE-RTX** ($c \approx 100$ μM) in the presence of DABCO (c = 10 mM) in MeCN are presented in Figure 5. Excitation of ***t*Bu-PE-RTX** results in fast intersystem crossing to the triplet state followed by an intermolecular electron transfer from DABCO to produce the radical ion pair with $\tau_{ET} \approx 40$ ns. The radical anion of the ***t*Bu-NI** station exhibits characteristic absorption bands at 419 and ~800 nm (Figure S29). The main absorption band of the radical anion (Figure 5) undergoes a time-dependent blue shift which has been shown to originate from the association of the **mc** with the ***t*Bu-NI** station.[47] The shuttling rate was determined by fitting the time-dependent peak position with a monoexponential function (solid line in Figure 5). The peak positions, indicated by markers in Figure 5, were obtained by fitting the spectra with a Gaussian band-shape function around the peak maximum. The shuttling rate in MeCN as determined from the UV–vis experiments is $1/k_{shuttling}$ = 143 ± 4 ns. The measurements were repeated with a higher concentration of DABCO (c = 60 mM), which yielded nearly an identical shuttling rate (Figure S30). The shuttling rate at the lower DABCO concentration in PhCN was, however, significantly smaller than that at higher DABCO concentration (780 ns vs 660 ns, Figures S31 and S32). This is most likely due to the relatively slow formation of the radical ion pairs (~200 ns) in more viscous PhCN. As the formation lifetime of the radical ion pairs approaches that of the shuttling, the processes become less distinguishable.

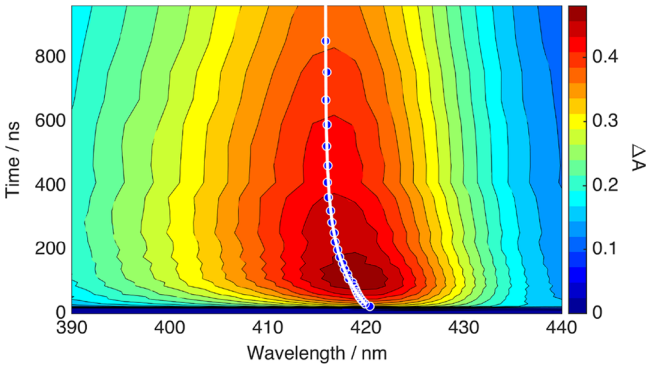

Figure 5. UV–vis transient absorption spectra of ***t*Bu-PE-RTX** ($c \approx 100$ μM) in the presence of DABCO (c = 10 mM). The peak maxima obtained from fits to a Gaussian line-shape function are indicated by the blue markers and the monoexponential fit of the peak maxima by the solid white line. Negative signals due to emissive processes are removed for clarity. The excitation wavelength was 355 nm.

Representative nanosecond UV–IR transient absorption spectra of ***t*Bu-PE-RTX** ($c \approx 100$ μM) in the presence of DABCO (c = 10 mM) in MeCN-d_3 are presented in Figure 6A.

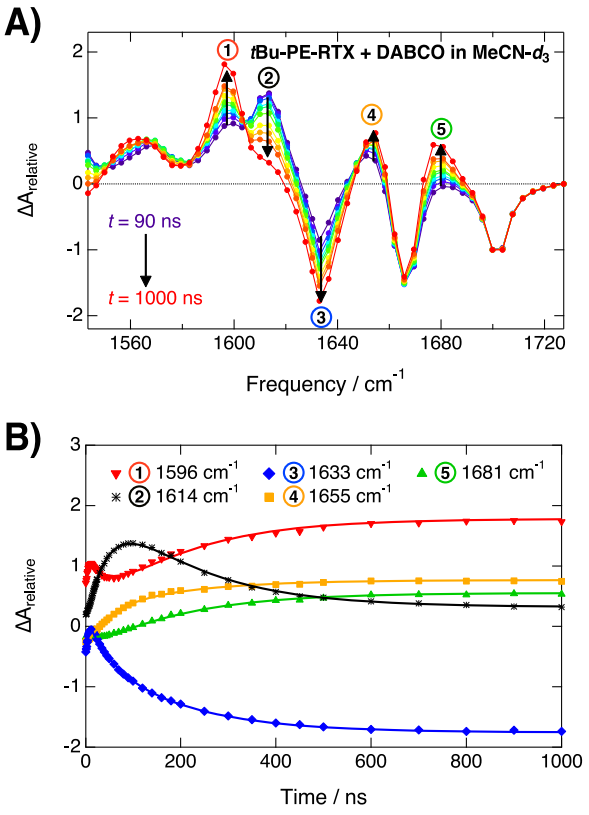

Figure 6. (A) UV–IR transient absorption spectra of ***t*Bu-PE-RTX** ($c \approx 100$ μM) in the presence of DABCO (c = 10 mM). The excitation wavelength was 355 nm. (B) Decay curves of the relevant absorption peaks indicated in (A). The solid lines represent the best fits with a global biexponential model at t > 10 ns.

The decay of the triplet state (t < 90 ns) is left out for clarity, and the first spectrum represents the transient spectrum of the radical anion. The spectra are normalized to the bleach of the symmetric CO-vibration peak at ~1700 cm^{-1}. The temporal behavior of this peak is determined only by the recombination of the radical ion pair. The normalization thus removes the contribution of the overall decay from the signal, and the observed spectral changes are solely due to the formation of the radical anion and the subsequent shuttling process.[66] A global fit of the five main peaks using a biexponential model described in the Supporting Information are presented in

DOI: 10.1021/jacs.9b10005
J. Am. Chem. Soc. 2019, 141, 19118–19129

Scheme 2. Schematic Representation of the Free Energy Landscapes of the Structurally Different Rotaxanes as a Function of the Shuttling Coordinate[a]

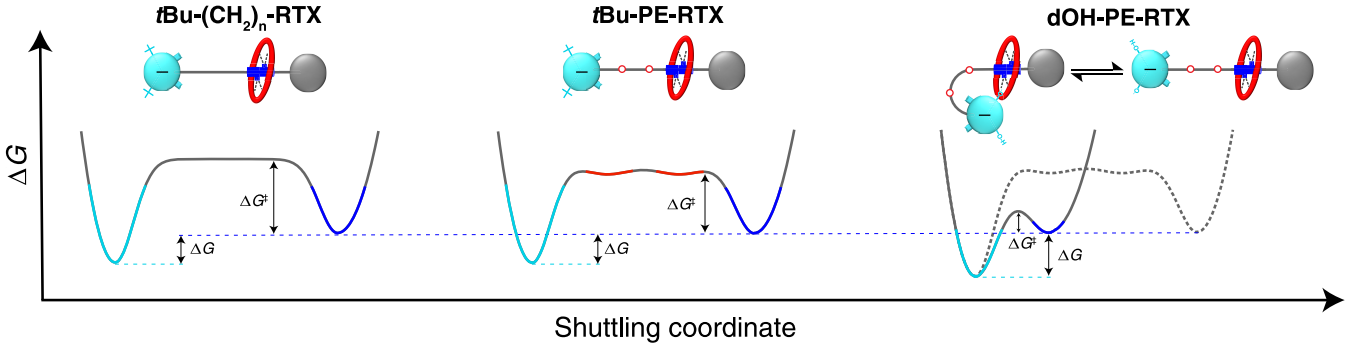

[a]The dashed free energy surface of **dOH-PE-RTX** (right) corresponds to the unfolded geometry, whereas the solid line represents that of the folded geometry.

Figure 6B. Further details on the analysis and interpretation of data can be found in ref 55.

Similarly to **dOH-PE-RTX**, the spectra exhibit ground-state bleach signals of the aromatic ring vibration (1633 cm^{-1}) and the antisymmetric (1666 cm^{-1}) and symmetric (1700 cm^{-1}) CO vibrations of the ***t*Bu-NI** station upon excitation. The strongest positive peak (peak 2, black) attributed to the symmetric CO vibration of the radical anion gradually shifts to a lower frequency (peak 1, red). This is attributed to the hydrogen bonding of the **mc** to the imide carbonyls of the ***t*Bu-NI** station. The increased hydrogen-bonding strength is also seen as induced absorption due to the shift of the amide I vibration of the **mc** (peak 4, orange). The departure of the **mc** is observed as a loss of the hydrogen-bonded **succ** vibration (1633 cm^{-1}, peak 3, blue) and appearance of the free **succ** vibration (1655 cm^{-1}, peak 5, green). Global fitting of the five main peaks yields a shuttling rate of $1/k_{shuttling}$ = 180 ± 10 ns, slightly longer than that observed in the UV−vis experiments. The slight differences in shuttling rates can be attributed to the different analysis methods and sample preparation conditions (see below). The shuttling time/rate constants are summarized in Table 2 and represent the average values from all the measurements (UV−vis and IR) and the errors are the corresponding standard deviations.

DISCUSSION

The aim of the study was to elaborate on the effect of the molecular composition of the different constituents on the shuttling speed and mechanism in hydrogen-bonded rotaxanes. All the shuttling time/rate constants are summarized in Table 2. A schematic representation of the energy landscapes of the structurally different rotaxanes as a function of the shuttling coordinate is presented in Scheme 2.

The shuttling rates of ***t*Bu-NI**-based rotaxanes with alkane threads have been previously studied in our group. Measurements on a series of rotaxanes with varying lengths of the alkane threads ($-(CH_2)_n-$ with n = 5, 9, 12, and 16) allowed us to propose a model that describes the rate as a function of the chain length.[55] Because the study did not include ***t*Bu-C_8-RTX**, the rate as predicted by the model was used in calculating the acceleration due to the introduction of oxygen atoms. Introduction of oxygen atoms in the thread increases the shuttling rate by ∼70% ($1/k_{shuttling}$ = 160 ns) compared to the predicted rate for ***t*Bu-C_8-RTX** ($1/k_{shuttling}$ = 270 ns). We believe that there can be two possible effects resulting in the faster shuttling.

First, the nearest oxygen atom to the **succ** station can facilitate the escape of the **mc** from the initial station. Instead of simultaneous breakage of four hydrogen bonds, the **mc** can break two hydrogen bonds from one side of the **succ** station and re-form two weaker hydrogen bonds to the nearest ether oxygen. This lowers the activation energy for the escape of the macrocycle (see Scheme 2), which is considered to be the rate-limiting step in the shuttling process.[55,57] A ∼70% acceleration in the shuttling rate is equal to a decrease of 0.3 kcal/mol in the free energy of activation. The decrease in free energy is comparable to differences in hydrogen-bond strengths between ether and carbonyl groups.[71] Jeppesen and Flood et al. also proposed that polyether threads assist in preparation of an early transition state lowering the total activation energy for the escape of the macrocycle, which supports our interpretation.[53]

The second possible effect for the acceleration could be the presence of minute amounts of water in the "dry" solvents.[72] Water has been shown to "lubricate" the shuttling process; that is, the rate is accelerated in the presence of water.[56] The acceleration was observed only at rather high concentrations of water (lowest studied concentration was 1 v/v %), but the study was done using ***t*Bu-C_{12}-RTX** that lacks oxygen atoms in the thread. Additional oxygen atoms offer a preferential hydrogen-bonding site for water molecules increasing the sensitivity. The shuttling rates determined from the time-resolved IR measurements were slightly smaller for both rotaxanes, which could indicate a lower residual water content. This can be attributed to differences in the sample preparation methods. The samples for the IR measurements were prepared in a glovebox, whereas a Schlenk technique under nitrogen flow was used for the UV−vis experiments.

dOH-PE-RTX exhibits surprisingly fast shuttling rates and, to the best of our knowledge, is the fastest photoswitchable molecular shuttle of this length scale reported to date. The polyether thread can only partially account for the observed acceleration. Therefore, we need to reconsider the shuttling mechanism. The fluorescence lifetime of the rotaxane in neat MeCN and PhCN is significantly shorter than those of the thread and the model **ref-dOH-NI** end station (see section S6, Supporting Information). This suggests that the macrocycle interacts with the **dOH-NI** end station, and the rotaxane is at least partly folded in its lowest-energy conformation. More-

DOI: 10.1021/jacs.9b10005
J. Am. Chem. Soc. 2019, 141, 19118−19129

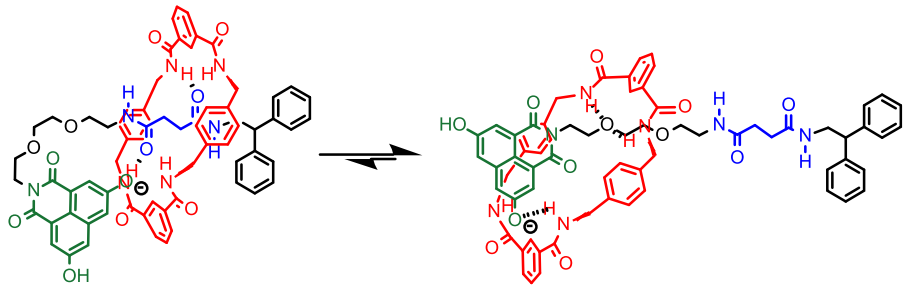

Figure 7. Alternative "harpooning" mechanism proposed for **dOH-PE-RTX**.

over, the oxygen atoms on the **PE** thread may induce bending of the thread facilitating the folding. Thus, it is reasonable to suggest that the shuttling also takes place in the folded state, significantly altering the free energy landscape as depicted in Scheme 2. The hydroxyl groups of the **dOH-NI** unit can hydrogen bond to the **mc** in the neutral form. After formation of the anion the **mc** can "slip" over the thread to hydrogen bond to deprotonated oxygen of the **dOH-NI** station. Such a "harpooning" mechanism has been already suggested for similar rotaxanes.[57] In this mechanism, the **mc** simultaneously hydrogen bonds to both stations in the transition state before departure from the initial station.

Another important difference between the two rotaxanes is the lack of clear changes in the imide carbonyl vibrations of **dOH-PE-RTX** upon shuttling compared to ***t*Bu-PE-RTX**, which exhibits a distinct red shift of symmetric CO-stretch vibration of the **NI** station upon arrival of the **mc** (peaks 1 and 2 in Figure 6). However, the spectra of both compounds exhibit distinct changes that can be attributed to the departure of **mc** from the **succ** station and increased hydrogen-bonding strength of the **mc** in the final state. In addition, the UV−vis spectra show a clear interaction between the macrocycle and the **dOH-NI** end station. Both of these observations strongly support our interpretation that the **mc** is translocated from the **succ** station to the **NI** end station. The difference between the two types of rotaxanes is the hydrogen-bonding geometry upon arrival of the **mc** to the **NI** station. In the case of **dOH-PE-RTX**, the **mc** hydrogen bonds mainly to the negatively charged deprotonated oxygen, which can be further stabilized by weaker hydrogen bonds to one of the carbonyl groups or to the ether oxygen. The blue shift of the UV−vis spectra observed for the **dOH-PE-RTX** anion is consistent with this because hydrogen bonding to the negatively charged oxygen results in a blue shift of the anion absorption band.[67] Moreover, the electron density in the deprotonated ground-state anion is largely localized on the aromatic oxygen, whereas in the radical anion of the ***t*Bu-NI** station, the negative charge is delocalized over the **NI** station with a significant density on the naphthalimide carbonyl groups.[47,64] A possible shuttling mechanism demonstrating both the folded geometry and hydrogen bonding to the deprotonated hydroxyl oxygen is presented in Figure 7. In this mechanism the deprotonated **NI** unit "pulls" the **mc** away from the **succ** station in a folded geometry and undergoes a conformational reorientation in the final state.

CONCLUSIONS

We have investigated the influence of the chemical structure of the constituent parts on the shuttling dynamics in two novel hydrogen-bonded rotaxanes. Comparison with previously reported compounds allowed us to separately study the effect of the thread and the end station on the shuttling rate and mechanism. Introduction of additional oxygen atoms on the thread of the previously studied ***t*Bu-NI**-based rotaxane[55] accelerates the shuttling by ∼70%. This is attributed to a decreased activation energy for the escape of the macrocycle from the initial station, which is considered to be the rate-limiting step in the shuttling process.[54] The additional oxygen atoms assist in preparation of an early transition state, where the macrocycle partially escapes the initial station and forms weaker hydrogen bonds to the nearest ether oxygen.

The shuttling of the macrocycle in **dOH-PE-RTX** is accelerated by a factor of ∼10, and to the best of our knowledge, it is the fastest photoswitchable molecular shuttle of this length scale (∼1 nm) reported to date. The shuttling in this rotaxane is proposed to take place in a folded conformation similar to the "harpooning" mechanism reported in the literature.[57] The hydrogen-bonding capability of the **dOH-NI** end station favors folding already in the initial state. Upon photochemical charging, the macrocycle can slip over the thread to hydrogen bond the end station, resulting in much faster shuttling speed. In addition, the macrocycle is assumed to mainly hydrogen bond to the negatively charged deprotonated hydroxyl group instead of the imide carbonyl groups observed for ***t*Bu-PE-RTX**.

Hydrogen-bond-donating and -accepting abilities of all constituting moieties have a direct and active effect on the shuttling dynamics. This is due to the competing interactions between the macrocycle, the stations, and the thread. Therefore, the shuttling mechanisms of chemically different hydrogen-bonded rotaxanes should be carefully evaluated and a derivation of a general mechanism may not be feasible. Our findings, however, contribute to the development and design of next generation photoswitchable [2]rotaxanes with increased shuttling rates and novel charging mechanisms.

EXPERIMENTAL SECTION

Synthesis. The synthesis of the novel **PE** thread compounds largely follows the previously reported procedures for the rotaxanes with all-alkane threads.[34,47,55] Instead of an alkane-based precursor, *tert*-butyl(2-(2-(2-aminoethoxy)ethoxy)ethyl)carbamate was used to for **PE** threads. The **dOH-NI**-based compounds were synthesized using a 3,6-dibenzoate-protected **NI** precursor. The final dihydroxy products were obtained after deprotection under basic conditions. Detailed synthetic procedures and characterizations are reported in the Supporting Information.

ASSOCIATED CONTENT

Supporting Information

The Supporting Information is available free of charge at https://pubs.acs.org/doi/10.1021/jacs.9b10005.

DOI: 10.1021/jacs.9b10005
J. Am. Chem. Soc. 2019, 141, 19118−19129

Details on materials, sample preparation, measurement techniques, and data analysis methods, demonstration of the spectral changes associated with the shuttling process, determination of the association constants from the absorption spectra, additional shuttling experiments, steady-state and time-resolved fluorescence experiments, synthesis, characterization, and NMR spectra of the target compounds (PDF)

AUTHOR INFORMATION

Corresponding Authors

*tatu.kumpulainen@unige.ch
*s.woutersen@uva.nl
*a.m.brouwer@uva.nl

ORCID

Tatu Kumpulainen: 0000-0001-9469-9294
Sander Woutersen: 0000-0003-4661-7738
Albert M. Brouwer: 0000-0002-1731-3869

Present Addresses

†Department of Physical Chemistry, Sciences II, University of Geneva, 30, Quai Ernest Ansermet, 1211 Geneva, Switzerland.
‡Department of Chemistry and Molecular Biology, University of Gothenburg, Medicinaregatan 9 C, 41390 Gothenburg, Sweden.

Notes

The authors declare no competing financial interest.

ACKNOWLEDGMENTS

The authors thank Hans Sanders for purification of some of the target compounds. This research was financially supported by The Netherlands Organization for Scientific Research (NWO) and the University of Amsterdam. T.K. acknowledges financial support from the Swiss National Science Foundation (SNSF, project PZ00P2_174116).

REFERENCES

(1) Browne, W. R.; Feringa, B. L. Making Molecular Machines Work. *Nat. Nanotechnol.* **2006**, *1*, 25−35.
(2) Kay, E. R.; Leigh, D. A. Beyond Switches: Rotaxane- and Catenane-Based Synthetic Molecular Motors. *Pure Appl. Chem.* **2008**, *80*, 17−29.
(3) Yang, W.; Li, Y.; Liu, H.; Chi, L.; Li, Y. Design and Assembly of Rotaxane-Based Molecular Switches and Machines. *Small* **2012**, *8*, 504−516.
(4) Wang, J., Ed. *Nanomachines: Fundamentals and Applications*; Wiley-VCH: Weinheim, Germany, 2013.
(5) Kay, E. R.; Leigh, D. A. Rise of the Molecular Machines. *Angew. Chem., Int. Ed.* **2015**, *54*, 10080−10088.
(6) Xue, M.; Yang, Y.; Chi, X.; Yan, X.; Huang, F. Development of Pseudorotaxanes and Rotaxanes: From Synthesis to Stimuli-Responsive Motions to Applications. *Chem. Rev.* **2015**, *115*, 7398−7501.
(7) Erbas-Cakmak, S.; Leigh, D. A.; McTernan, C. T.; Nussbaumer, A. L. Artificial Molecular Machines. *Chem. Rev.* **2015**, *115*, 10081−10206.
(8) Colasson, B.; Credi, A.; Ragazzon, G. Light-Driven Molecular Machines Based on Ruthenium(II) Polypyridine Complexes: Strategies and Recent Advances. *Coord. Chem. Rev.* **2016**, *325*, 125−134.
(9) Kassem, S.; van Leeuwen, T.; Lubbe, A. S.; Wilson, M. R.; Feringa, B. L.; Leigh, D. A. Artificial Molecular Motors. *Chem. Soc. Rev.* **2017**, *46*, 2592−2621.
(10) Baroncini, M.; Casimiro, L.; de Vet, C.; Groppi, J.; Silvi, S.; Credi, A. Making and Operating Molecular Machines: A Multidisciplinary Challenge. *ChemistryOpen* **2018**, *7*, 169−179.
(11) Zhang, L.; Marcos, V.; Leigh, D. A. Molecular Machines with Bio-inspired Mechanisms. *Proc. Natl. Acad. Sci. U. S. A.* **2018**, *115*, 9397−9404.
(12) Baroncini, M.; Silvi, S.; Credi, A. Photo- and Redox-Driven Artificial Molecular Motors. *Chem. Rev.* **2019**, DOI: 10.1021/acs.chemrev.9b00291.
(13) Feringa, B. L., Ed. *Molecular Switches*, 2nd ed.; Wiley-VCH: Weinheim, Germany, 2001.
(14) Choi, J. W.; Flood, A. H.; Steuerman, D. W.; Nygaard, S.; Braunschweig, A. B.; Moonen, N. N. P.; Laursen, B. W.; Luo, Y.; DeIonno, E.; Peters, A. J.; Jeppesen, J. O.; Xu, K.; Stoddart, J. F.; Heath, J. R. Ground-State Equilibrium Thermodynamics and Switching Kinetics of Bistable [2]Rotaxanes Switched in Solution, Polymer Gels, and Molecular Electronic Devices. *Chem. - Eur. J.* **2006**, *12*, 261−279.
(15) Gust, D.; Moore, T. A.; Moore, A. L. Molecular Switches Controlled by Light. *Chem. Commun.* **2006**, 1169−1178.
(16) Green, J. E.; Wook Choi, J.; Boukai, A.; Bunimovich, Y.; Johnston-Halperin, E.; DeIonno, E.; Luo, Y.; Sheriff, B. A.; Xu, K.; Shik Shin, Y.; Tseng, H.-R.; Stoddart, J. F.; Heath, J. R. 160-Kilobit Molecular Electronic Memory Patterned at 10^{11} Bits per Square Centimetre. *Nature* **2007**, *445*, 414−417.
(17) Harada, A. Cyclodextrin-Based Molecular Machines. *Acc. Chem. Res.* **2001**, *34*, 456−464.
(18) Collin, J.-P.; Dietrich-Buchecker, C.; Gaviña, P.; Jimenez-Molero, M. C.; Sauvage, J.-P. Shuttles and Muscles: Linear Molecular Machines Based on Transition Metals. *Acc. Chem. Res.* **2001**, *34*, 477−487.
(19) Kay, E. R.; Leigh, D. A.; Zerbetto, F. Synthetic Molecular Motors and Mechanical Machines. *Angew. Chem., Int. Ed.* **2007**, *46*, 72−191.
(20) Hirose, K.; Shiba, Y.; Ishibashi, K.; Doi, Y.; Tobe, Y. A Shuttling Molecular Machine with Reversible Brake Function. *Chem. - Eur. J.* **2008**, *14*, 3427−3433.
(21) Li, H.; Li, X.; Wu, Y.; Agren, H.; Qu, D.-H. A Musclelike [2](2)Rotaxane: Synthesis, Performance, and Molecular Dynamics Simulations. *J. Org. Chem.* **2014**, *79*, 6996−7004.
(22) Waeles, P.; Riss-Yaw, B.; Coutrot, F. Synthesis of a pH-Sensitive Hetero[4]Rotaxane Molecular Machine that Combines [c2]Daisy and [2]Rotaxane Arrangements. *Chem. - Eur. J.* **2016**, *22*, 6837−6845.
(23) Moretto, A.; Menegazzo, I.; Crisma, M.; Shotton, E. J.; Nowell, H.; Mammi, S.; Toniolo, C. A Rigid Helical Peptide Axle for a [2]Rotaxane Molecular Machine. *Angew. Chem., Int. Ed.* **2009**, *48*, 8986−8989.
(24) Berná, J.; Alajarín, M.; Marín-Rodríguez, C.; Franco-Pujante, C. Redox Divergent Conversion of a [2]Rotaxane into two Distinct Degenerate Partners with Different Shuttling Dynamics. *Chem. Sci.* **2012**, *3*, 2314−2320.
(25) Waeles, P.; Fournel-Marotte, K.; Coutrot, F. Distinguishing Two Ammonium and Triazolium Sites of Interaction in a Three-Station [2]Rotaxane Molecular Shuttle. *Chem. - Eur. J.* **2017**, *23*, 11529−11539.
(26) Astumian, R. D. Design Principles for Brownian Molecular Machines: How to Swim in Molasses and Walk in a Hurricane. *Phys. Chem. Chem. Phys.* **2007**, *9*, 5067−5083.
(27) Bauer, W. R.; Nadler, W. Dynamics and Efficiency of Brownian Rotors. *J. Chem. Phys.* **2008**, *129*, 225103.
(28) Badjić, J. D.; Balzani, V.; Credi, A.; Silvi, S.; Stoddart, J. F. A Molecular Elevator. *Science* **2004**, *303*, 1845−1849.
(29) Marlin, D. S.; González Cabrera, D.; Leigh, D. A.; Slawin, A. M. Z. Complexation-Induced Translational Isomerism: Shuttling through Stepwise Competitive Binding. *Angew. Chem., Int. Ed.* **2006**, *45*, 77−83.

DOI: 10.1021/jacs.9b10005
J. Am. Chem. Soc. 2019, 141, 19118−19129

(30) Cheng, K.-W.; Lai, C.-C.; Chiang, P.-T.; Chiu, S.-H. Reading the Operation of an Acid/Base-Controllable Molecular Switch by Naked Eye. *Chem. Commun.* **2006**, 2854−2856.
(31) Keaveney, C. M.; Leigh, D. A. Shuttling Through Anion Recognition. *Angew. Chem., Int. Ed.* **2004**, *43*, 1222−1224.
(32) Zhou, W.; Wu, Y.; Zhai, B.-Q.; Wang, Q.-C.; Qu, D.-H. An anthracene-containing bistable [2]rotaxane featuring color and fluorescence changes. *RSC Adv.* **2014**, *4*, 5148−5151.
(33) Ragazzon, G.; Credi, A.; Colasson, B. Thermodynamic Insights on a Bistable Acid−Base Switchable Molecular Shuttle with Strongly Shifted Co-conformational Equilibria. *Chem. - Eur. J.* **2017**, *23*, 2149−2156.
(34) Altieri, A.; Gatti, F. G.; Kay, E. R.; Leigh, D. A.; Martel, D.; Paolucci, F.; Slawin, A. M. Z.; Wong, J. K. Y. Electrochemically Switchable Hydrogen-Bonded Molecular Shuttles. *J. Am. Chem. Soc.* **2003**, *125*, 8644−8654.
(35) Bruns, C. J.; Frasconi, M.; Iehl, J.; Hartlieb, K. J.; Schneebeli, S. T.; Cheng, C.; Stupp, S. I.; Stoddart, J. F. Redox Switchable Daisy Chain Rotaxanes Driven by Radical-Radical Interactions. *J. Am. Chem. Soc.* **2014**, *136*, 4714−4723.
(36) Yasuda, T.; Tanabe, K.; Tsuji, T.; Coti, K. K.; Aprahamian, I.; Stoddart, J. F.; Kato, T. A Redox-Switchable [2]Rotaxane in a Liquid-Crystalline State. *Chem. Commun.* **2010**, *46*, 1224−1226.
(37) Balzani, V.; Clemente-León, M.; Credi, A.; Ferrer, B.; Venturi, M.; Flood, A. H.; Stoddart, J. F. Autonomous Artificial Nanomotor Powered by Sunlight. *Proc. Natl. Acad. Sci. U. S. A.* **2006**, *103*, 1178−1183.
(38) Saha, S.; Stoddart, J. F. Photo-Driven Molecular Devices. *Chem. Soc. Rev.* **2007**, *36*, 77−92.
(39) Silvi, S.; Venturi, M.; Credi, A. Light Operated Molecular Machines. *Chem. Commun.* **2011**, *47*, 2483−2489.
(40) Leigh, D. A.; Marcos, V.; Nalbantoglu, T.; Vitorica-Yrezabal, I. J.; Yasar, F. T.; Zhu, X. Pyridyl-Acyl Hydrazone Rotaxanes and Molecular Shuttles. *J. Am. Chem. Soc.* **2017**, *139*, 7104−7109.
(41) Yu, J.-J.; Zhao, L.-Y.; Shi, Z.-T.; Zhang, Q.; London, G.; Liang, W.-J.; Gao, C.; Li, M.-M.; Cao, X.-M.; Tian, H.; Feringa, B. L.; Qu, D.-H. Pumping a Ring-Sliding Molecular Motion by a Light-Powered Molecular Motor. *J. Org. Chem.* **2019**, *84*, 5790−5802.
(42) Ballardini, R.; Balzani, V.; Credi, A.; Gandolfi, M. T.; Venturi, M. Artificial Molecular-Level Machines: Which Energy To Make Them Work? *Acc. Chem. Res.* **2001**, *34*, 445−455.
(43) Pezzato, C.; Cheng, C.; Stoddart, J. F.; Astumian, R. D. Mastering the Non-equilibrium Assembly and Operation of Molecular Machines. *Chem. Soc. Rev.* **2017**, *46*, 5491−5507.
(44) Yan, H.; Zhu, L.; Li, X.; Kwok, A.; Li, X.; Agren, H.; Zhao, Y. Photothermal-Responsive [2]Rotaxanes. *RSC Adv.* **2013**, *3*, 2341−2350.
(45) Baroncini, M.; Silvi, S.; Venturi, M.; Credi, A. Photoactivated Directionally Controlled Transit of a Non-Symmetric Molecular Axle Through a Macrocycle. *Angew. Chem., Int. Ed.* **2012**, *51*, 4223−4226.
(46) Baroncini, M.; Silvi, S.; Venturi, M.; Credi, A. Reversible Photoswitching of Rotaxane Character and Interplay of Thermodynamic Stability and Kinetic Lability in a Self-Assembling Ring−Axle Molecular System. *Chem. - Eur. J.* **2010**, *16*, 11580−11587.
(47) Brouwer, A. M.; Frochot, C.; Gatti, F. G.; Leigh, D. A.; Mottier, L.; Paolucci, F.; Roffia, S.; Wurpel, G. W. H. Photoinduction of Fast, Reversible Translational Motion in a Hydrogen-Bonded Molecular Shuttle. *Science* **2001**, *291*, 2124−2128.
(48) Saha, S.; Flood, A. H.; Stoddart, J. F.; Impellizzeri, S.; Silvi, S.; Venturi, M.; Credi, A. A Redox-Driven Multicomponent Molecular Shuttle. *J. Am. Chem. Soc.* **2007**, *129*, 12159−12171.
(49) Examples of utilization of photoinduced proton release as a trigger mechanism for molecular machines and switches exist in the literature. However, all reported examples are based on either irreversible photoacid generators or metastable state photoacids. Utilization of conventional excited-state acids has not been demonstrated. See ref 12 for a recent review on photoswitchable molecular machines.
(50) Choi, J. W.; Flood, A. H.; Steuerman, D. W.; Nygaard, S.; Braunschweig, A. B.; Moonen, N.; Laursen, B. W.; Luo, Y.; DeIonno, E.; Peters, A. J.; Jeppesen, J. O.; Xu, K.; Stoddart, J. F.; Heath, J. R. Ground-State Equilibrium Thermodynamics and Switching Kinetics of Bistable [2]Rotaxanes Switched in Solution, Polymer Gels, and Molecular Electronic Devices. *Chem. - Eur. J.* **2006**, *12*, 261−279.
(51) Avellini, T.; Li, H.; Coskun, A.; Barin, G.; Trabolsi, A.; Basuray, A. N.; Dey, S. K.; Credi, A.; Silvi, S.; Stoddart, J. F.; Venturi, M. Photoinduced Memory Effect in a Redox Controllable Bistable Mechanical Molecular Switch. *Angew. Chem., Int. Ed.* **2012**, *51*, 1611−1615.
(52) Nygaard, S.; Laursen, B. W.; Flood, A. H.; Hansen, C. N.; Jeppesen, J. O.; Stoddart, J. F. Quantifying the Working Stroke of Tetrathiafulvalene-Based Electrochemically-Driven Linear Motor-Molecules. *Chem. Commun.* **2006**, 144−146.
(53) Andersen, S. S.; Share, A. I.; Poulsen, B. L. C.; Kørner, M.; Duedal, T.; Benson, C. R.; Hansen, S. W.; Jeppesen, J. O.; Flood, A. H. Mechanistic Evaluation of Motion in Redox-Driven Rotaxanes Reveals Longer Linkers Hasten Forward Escapes and Hinder Backward Translations. *J. Am. Chem. Soc.* **2014**, *136*, 6373−6384.
(54) Young, P. G.; Hirose, K.; Tobe, Y. Axle Length Does Not Affect Switching Dynamics in Degenerate Molecular Shuttles with Rigid Spacers. *J. Am. Chem. Soc.* **2014**, *136*, 7899−7906.
(55) Panman, M. R.; Bodis, P.; Shaw, D. J.; Bakker, B. H.; Newton, A. C.; Kay, E. R.; Brouwer, A. M.; Buma, W. J.; Leigh, D. A.; Woutersen, S. Operation Mechanism of a Molecular Machine Revealed Using Time-Resolved Vibrational Spectroscopy. *Science* **2010**, *328*, 1255−1258.
(56) Panman, M. R.; Bakker, B. H.; den Uyl, D.; Kay, E. R.; Leigh, D. A.; Buma, W. J.; Brouwer, A. M.; Geenevasen, J. A. J.; Woutersen, S. Water Lubricates Hydrogen-Bonded Molecular Machines. *Nat. Chem.* **2013**, *5*, 929−934.
(57) Baggerman, J.; Haraszkiewicz, N.; Wiering, P. G.; Fioravanti, G.; Marcaccio, M.; Paolucci, F.; Kay, E. R.; Leigh, D. A.; Brouwer, A. M. Induction of Motion in a Synthetic Molecular Machine: Effect of Tuning the Driving Force. *Chem. - Eur. J.* **2013**, *19*, 5566−5577.
(58) Panman, M. R.; van Dijk, C. N.; Huerta-Viga, A.; Sanders, H. J.; Bakker, B. H.; Leigh, D. A.; Brouwer, A. M.; Buma, W. J.; Woutersen, S. Transient Two-Dimensional Vibrational Spectroscopy of an Operating Molecular Machine. *Nat. Commun.* **2017**, *8*, 2206.
(59) Jagesar, D. C.; Fazio, S. M.; Taybi, J.; Eiser, E.; Gatti, F. G.; Leigh, D. A.; Brouwer, A. M. Photoinduced Shuttling Dynamics of Rotaxanes in Viscous Polymer Solutions. *Adv. Funct. Mater.* **2009**, *19*, 3440−3449.
(60) Günbaş, D. D.; Brouwer, A. M. Degenerate molecular shuttles with flexible and rigid spacers. *J. Org. Chem.* **2012**, *77*, 5724−5735.
(61) Günbaş, D. D.; Zalewski, L.; Brouwer, A. M. Energy Landscape of a Hydrogen-Bonded Non-degenerate Molecular Shuttle. *Chem. Commun.* **2010**, *46*, 2061−2063.
(62) Gholami, G.; Zhu, K.; Baggi, G.; Schott, E.; Zarate, X.; Loeb, S. J. Influence of Axle Length on the Rate and Mechanism of Shuttling in Rigid H-shaped [2]Rotaxanes. *Chem. Sci.* **2017**, *8*, 7718−7723.
(63) Ogoshi, T.; Kotera, D.; Nishida, S.; Kakuta, T.; Yamagishi, T.-A.; Brouwer, A. M. Spacer Length-Independent Shuttling of the Pillar[5]arene Ring in Neutral [2]Rotaxanes. *Chem. - Eur. J.* **2018**, *24*, 6325−6329.
(64) Kumpulainen, T.; Bakker, B. H.; Brouwer, A. M. Complexes of a Naphthalimide Photoacid with Organic Bases, and Their Excited-State Dynamics in Polar Aprotic Organic Solvents. *Phys. Chem. Chem. Phys.* **2015**, *17*, 20715−20724.
(65) Wurpel, G. W. H. Photoinduced Dynamics in Hydrogen-Bonded Rotaxanes. Ph.D. thesis, University of Amsterdam, 2001.
(66) Panman, M. R. Observing Invisible Machines with Invisible Light. Ph.D. thesis, University of Amsterdam, 2013.
(67) Kumpulainen, T.; Rosspeintner, A.; Dereka, B.; Vauthey, E. Influence of Solvent Relaxation on Ultrafast Excited-State Proton Transfer to Solvent. *J. Phys. Chem. Lett.* **2017**, *8*, 4516−4521.
(68) Ragazzon, G.; Schäfer, C.; Franchi, P.; Silvi, S.; Colasson, B.; Lucarini, M.; Credi, A. Remote Electrochemical Modulation of p*K*a in

DOI: 10.1021/jacs.9b10005
J. Am. Chem. Soc. 2019, 141, 19118−19129

a Rotaxane by Co-conformational Allostery. *Proc. Natl. Acad. Sci. U. S. A.* **2018**, *115*, 9385−9390.
(69) Panman, M. R.; Bodis, P.; Shaw, D. J.; Bakker, B. H.; Newton, A. C.; Kay, E. R.; Leigh, D. A.; Buma, W. J.; Brouwer, A. M.; Woutersen, S. Time-Resolved Vibrational Spectroscopy of a Molecular Shuttle. *Phys. Chem. Chem. Phys.* **2012**, *14*, 1865−1875.
(70) Jagesar, D. C.; Hartl, F.; Buma, W. J.; Brouwer, A. M. Infrared Study of Intercomponent Interactions in a Switchable Hydrogen-Bonded Rotaxane. *Chem. - Eur. J.* **2008**, *14*, 1935−1946.
(71) Lommerse, J. P. M.; Price, S. L.; Taylor, R. Hydrogen Bonding of Carbonyl, Ether, and Ester Oxygen Atoms with Alkanol Hydroxyl Groups. *J. Comput. Chem.* **1997**, *18*, 757−774.
(72) Williams, D. B. G.; Lawton, M. Drying of Organic Solvents: Quantitative Evaluation of the Efficiency of Several Desiccants. *J. Org. Chem.* **2010**, *75*, 8351−8354.

DOI: 10.1021/jacs.9b10005
J. Am. Chem. Soc. 2019, 141, 19118−19129